ACS APPLIED MATERIALS & INTERFACES

www.acsami.org

Research Article

Textile Triboelectric Nanogenerators Simultaneously Harvesting Multiple "High-Entropy" Kinetic Energies

Xuechao Gang, Zi Hao Guo, Zifeng Cong, Jing Wang, Caiyun Chang, Chongxiang Pan, Xiong Pu,* and Zhong Lin Wang*

Cite This: *ACS Appl. Mater. Interfaces* 2021, 13, 20145−20152

Read Online

ACCESS | Metrics & More | Article Recommendations | Supporting Information

ABSTRACT: Distributed renewable kinetic energies are ubiquitous but with irregular amplitudes and frequencies, which, as one category of "high-entropy" energies, are crucial for next-generation self-powered electronics. Herein, we present a flexible waterproof dual-mode textile triboelectric nanogenerator (TENG), which can simultaneously scavenge multiple "high-entropy" kinetic energies, including human motions, raindrops, and winds. A freestanding-mode textile TENG (F-TENG) and a contact-separation-mode textile TENG (CS-TENG) are integrated together. The structure parameters of the textile TENG are optimized to improve the output performances. The raindrop can generate a voltage of up to ∼4.3 V and a current of about ∼6 μA, while human motion can generate a voltage of over 120 V and a peak power density of ∼500 mW m^{-2}. The scavenged electrical energies can be stored in capacitors for powering small electronics. Therefore, we demonstrated a facile preparation of a TENG-based energy textile that is highly promising for kinetic energy harvesting and self-powered electronics.

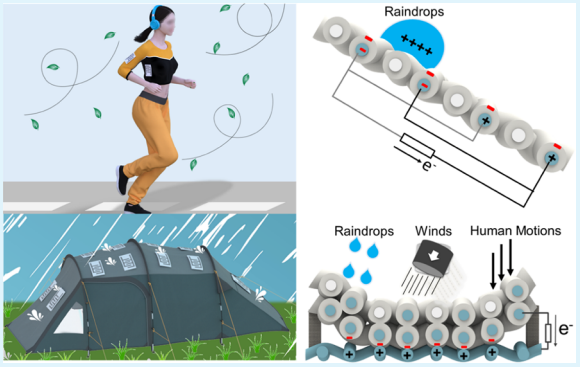

KEYWORDS: *textile, triboelectric nanogenerator, wind, raindrop, human motion, energy harvesting*

1. INTRODUCTION

Distributed renewable energies will play increasingly important roles along with the implementation of new technologies like the internet of things, artificial intelligence, and wearable electronics.[1−4] Various types of smart terminals are indispensable to support these technologies, which, however, are all almost impossible to power by conventional electric power transmitted by electric lines due to their gigantic quantities and wide distributions. Harvesting energies from their working environments is becoming an alternative. Nevertheless, these energies, either solar, thermal, chemical, or kinetic,[5−7] are typically irregular in time, random in physical space, and wasted in most cases, which are therefore termed "high-entropy" energies.[8] It still remains a challenge to efficiently harvest these energies and to integrate the energy harvesters into self-powered smart electronics.

Mechanical kinetic energies are free, clean, and ubiquitous. Triboelectric nanogenerators (TENGs) have been recently developed for harvesting various types of mechanical energies, including human motions, vibrations, winds, water drop, and so on.[9−12] The TENG converts mechanical energy into electricity based on the effects of contact electrification and electrostatic induction, and four basic working modes have been developed.[13] It has been found that TENGs outweigh the traditional electromagnetic generators when the motion frequency is low (<5 Hz) and the motion amplitude is low.[14] Furthermore, the abundant choices of materials and versatility in structure designs make TENGs potentially flexible, stretchable, transparent, self-healable, etc.[15−17] Therefore, intensive efforts are being made to investigate multifunctional TENGs, aiming as power sources of various wearable electronics.[18,19]

Among different multifunctional TENGs, textile-based TENGs are of special interest. Smart electronic textiles are promising candidates for achieving comfortable wearable electronics,[20−22] but the development of compatible energy devices is still a bottleneck for their practical applications. Textile TENGs can utilize common natural or synthetic yarn materials to construct power devices while maintaining the flexibility, breathability, and even washability of common textiles.[23−27] Intensive research has been carried out to fabricate textile TENGs to harvest human motion energies. Several studies also reported hybrid power textiles that can harvest multiple energies (human motion and solar energies) using textile TENGs and solar cells.[28,29] Nevertheless,

Received: February 18, 2021
Accepted: April 8, 2021
Published: April 20, 2021

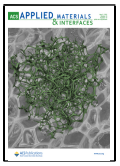

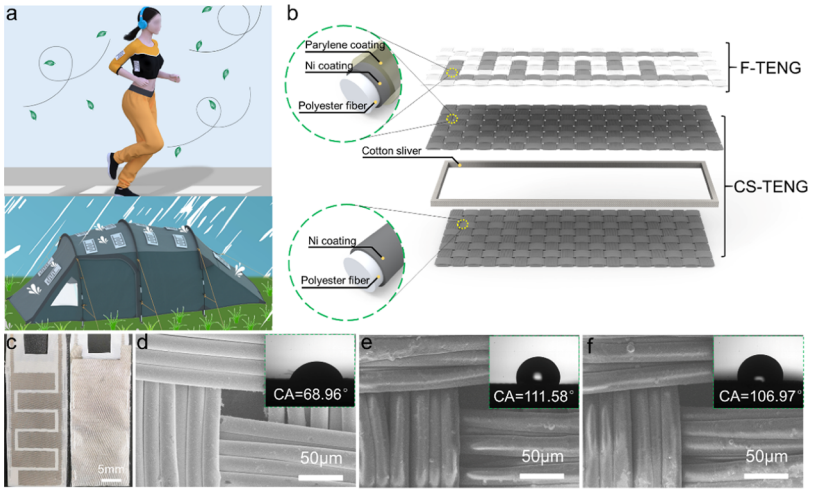

Figure 1. Design and fabrication of the dual-mode textile TENG. (a) Schematic illustration of the possible applications of the dual-mode TENG in smart cloths or tents for scavenging multiple "high-entropy" kinetic energies (raindrops, winds, or human motions). (b) Schematic diagram of the fabricated dual-mode TENG. (c) Photograph of both sides of the dual-mode textile TENG. SEM and contact angle images of Ni-coated fabrics (d) before and (e) after being coated with an insulating Parylene film. (f) SEM and contact angle images of Parylene/Ni-coated fabrics after performing the water repellent test three times.

considering that the TENG itself can scavenge different types of kinetic energies,[30−33] it is possible to construct a textile TENG for harvesting multiple environmental energies, such as human motions, water drops, and wind energy. Despite several preliminary attempts,[34] further investigations are still required of textile TENGs capable of harvesting multiple energies to optimize their fabrication, structures, and performances.

Herein, we present a flexible waterproof dual-mode textile TENG that can simultaneously scavenge multiple "high-entropy" mechanical energies, including human motions, raindrops, and winds. The dual-mode TENG consists of a contact-separation-mode TENG (CS-TENG) for harvesting mechanical energy from raindrops, winds, and human motions, and a freestanding-mode TENG (F-TENG) with interdigitated electrodes for collecting the kinetic energy of raindrops. Specifically, a route of laser-scribing masking and electroless deposition (ELD) was developed for the fabrication of interdigitated F-TENG textiles. Furthermore, F-TENG and CS-TENG were integrated together into a single cloth by a sewing method. The influencing parameters on the electrical output performances of the TENG have been systematically studied, especially for the F-TENG. The raindrop can generate a voltage of up to ∼4.3 V and current of about ∼6 μA, while human motion can generate a voltage of over 120 V and a peak power density of ∼500 mW m^{-2}. The scavenged electrical energies could be stored in capacitors for powering small electronics. Therefore, we demonstrated a facile preparation of a textile TENG-based energy device that can simultaneously harvest multiple kinetic energies.

2. RESULTS AND DISCUSSION

2.1. Design and Fabrication of the Textile TENGs. Figure 1a shows our proposed dual-mode textile TENG that can simultaneously scavenge multiple "high-entropy" mechanical energies, including human motions, raindrops, and winds. It is possible to integrate it in a smart cloth, a tent, or some other outdoor facilities. The structure of the fabricated textile TENG is schematically illustrated in Figure 1b, which consists of an F-TENG on the top and a CS-TENG on the bottom. The F-TENG has a coplanar structure with two interdigitated electrodes. The two interdigitated electrodes were electroless-deposited Ni on a polyester fabric, on top of which a Parylene film was conformally coated to serve as the triboelectrification layer. The fabrication of this textile F-TENG was similar to our previous work.[25] A Kapton mask produced using a laser scriber was employed to aid the fabrication of patterned Ni coatings on the fabrics. The Parylene film was coated using a chemical vapor deposition (CVD) method. The interval gap between adjacent finger electrodes was 2 mm to ensure electrical disconnection, while the width of a finger electrode unit was varied for optimization. This F-TENG can be utilized to scavenge the kinetic energy of water drops sliding on the top. The CS-TENG underneath the F-TENG consists of two fabrics separated by a cotton fabric strip as the spacer. One of the fabrics is a conductive Ni-coated polyester textile; the other is a polyester textile coated with Ni and a Parylene film. Therefore, the vertical contact-separation motion between these two fabrics will generate static charges on the Parylene film and induce current flow between the two Ni coating electrodes. This CS-TENG can therefore harvest kinetic energies from water drops, winds, and human motions, which will be discussed hereafter. These two textile TENGs were sewed together with the F-TENG on the top, as shown by the photograph in Figure 1c. The dual-mode TENG can be easily bent, wrapped, and immersed in water without damage, indicating their excellent flexibility and washability. The TENG textiles were completely folded to 180° 100 times, washed for 30 min, and then dried (Figure S1a−c). The V_{oc} with a linear motor to mimic body movements shows no significant decrease after undergoing these harsh deformations (Figure S1d), confirming that the dual-mode TENG is flexible and washable. Furthermore, the dual-mode TENG showed slightly lower air permeability (80.76 mm s^{-1}) than trilaminar polyester fabrics (133.87 mm s^{-1}) (Figure S1e).

The SEM images of Ni-coated fabrics before (Figure 1d) and after (Figure 1e) being coated with an insulating Parylene film confirmed that both the electroless-deposited Ni coatings and the CVD-coated Parylene films maintained the woven structure of the pristine textile, which helps in maintaining the flexibility and breathability of the TENG fabrics. The top

https://doi.org/10.1021/acsami.1c03250
ACS Appl. Mater. Interfaces 2021, 13, 20145−20152

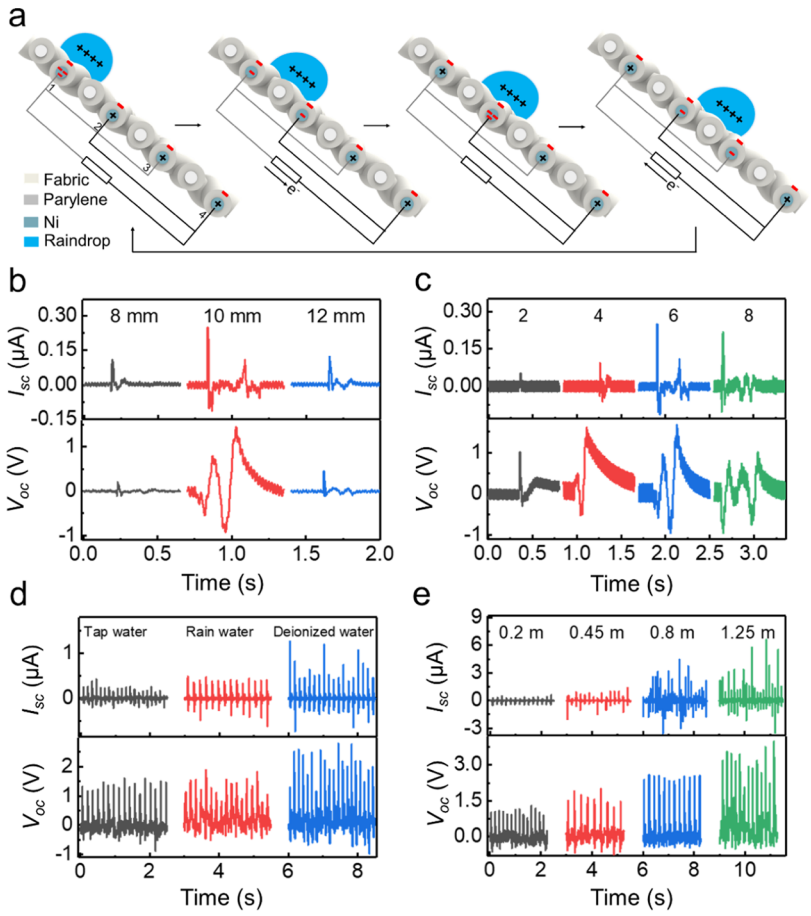

Figure 2. Harvesting raindrop energy by F-TENG. (a) Schematic illustration of the working mechanism of F-TENG for raindrop energy harvesting. Dependence of I_{sc} and V_{oc} on (b) the electrode width, (c) the total number (n) of electrode fingers, (d) types of water droplets, and (e) raindrop fall height.

Parylene layer was hydrophobic (the contact angle is 111.58°, as shown in the inset of Figure 1e), which is crucial for harvesting water drop energies. The water drop has to roll or slide on the textile rather than spread or soak in the textile, so that the contact electrification can happen between water drops and the fabric surfaces. Furthermore, the top F-TENG should be water repellent, so that the water will not penetrate to the underneath CS-TENG. Otherwise, the two electrodes of the CS-TENG will be shortened. A water repellent test of fabrics based on the standard test method AATCC42-2007 illustrated that the Ni fabric coated with insulating Parylene was waterproof (Figure S2). An absorbent paper underneath the fabric showed almost no weight increase after striking the fabric with water drops from 0.6 m height for 5 min. The morphology of the fabric showed no change, and the water contact angle showed a slight decrease after the water repellent test was performed three times (Figure 1f).

2.2. Harvesting Raindrop Energies. The schematic diagram of the working principle of F-TENG for raindrop energy harvesting is depicted in Figure 2a. For simplification, four adjacent finger electrodes and a single raindrop were taken as an example to illustrate the dynamic process of energy conversion. Previous reports have shown that contact electrification with air, aerosols, or tubes can induce electrostatic charges in water, and the polarity of the charge on the water drop surface relies on the materials that it comes into contact with.[35−37] A recent study even found that the electron-transfer behavior between the water drop and the contacting surfaces dominates the generation of electrostatic charges.[38] Generally, the water drop will be positively charged when dropping from the air.[39] Furthermore, when it makes contact with the Parylene film, contact electrification will further increase positive charges in the droplet, while negative static charges are produced in the Parylene film.[40] After striking the Parylene-coated textile with water drops for a certain time period, the Parylene layer will be negatively charged, which was electrically screened by inducing positive charges in the Ni electrodes. When a positively charged water drop slides down on the Parylene surface, their unscreened positive charges will further induce extra negative charges in the Ni electrodes, and therefore will cause current to flow through the external load between the two finger electrodes, to achieve local charge equilibrium. As finger electrode 1 and finger electrode 2 are alternatingly adjacent to each other, a pulsed alternating current (AC) will be generated when water drops keep sliding on the F-TENG textile.

A homemade spray head was used to spray water drops from a certain height (see Figure S3) and investigate the electric output of the F-TENG. We first simply used tap water for the experiment, and the water drops fell independently onto the textile surface. The dependences of short-circuit current (I_{sc}) and open-circuit voltage (V_{oc}) on the electrode width are shown in Figure 2b. Note that we tilted the F-TENG device to 50° to make the water drops flow along the upper surface of F-

https://doi.org/10.1021/acsami.1c03250
ACS Appl. Mater. Interfaces 2021, 13, 20145−20152

TENG, and the droplet size was constant. It is found that the current and voltage are the highest when the width is close to the droplet size (9.8 mm, measured by fixing a droplet on the F-TENG textile). It is easy to understand that no current flows through the external circuit if a droplet covers both the adjacent electrodes, while if the droplet is far smaller than the electrode, its sliding motion cannot immediately break the local charge equilibrium or induce the charge flow between the two electrodes. In a real situation, several F-TENGs with different electrode widths can be integrated together since the raindrop size may vary (about 0.5−5.5 mm). The total number (n) of electrode fingers of the two interdigitated electrodes was also varied. The current and voltage outputs for a single droplet sliding down the textile surface are shown in Figure 2c. When the total finger number was two, only a single current and voltage peak was observed since the droplet position changed only once between the two electrodes. Increasing the finger number leads to an increase in the number of current and voltage peaks. Strictly speaking, there should be $(n - 1)$ current or voltage peaks, but the observed peak number was slightly smaller. This is possibly due to the dissipation of the charges in the droplet during sliding motions, as it can be confirmed that the current peak height was decreasing for each sliding motion.

To mimic the actual situation of raindrops, the electricity generated from different types of water droplets was also compared. The rainwater was home-made by mixing deionized water, a small amount of sulfur dioxide, nitrogen dioxide, impurities, and floating dust, which has a pH value of 5.7. It was found that the deionized water exhibited the highest output (~0.8 μA and ~3.3 V), as shown in Figure 2d. The higher capability of deionized water in contact electrification has also been observed in other previous reports.[41,42] The charge transfer between deionized water and polymer is dominated by electron transfer. As the concentration of ions in the aqueous solution increases, the ions accumulate at the liquid−solid interface, hindering the electron-transfer process due to the screening effect. Therefore, the contact electrification (CE) between the ionic solution and polymer has both ion transfer and electron transfer, while the charge transfer between nonionic liquid and polymer is substantially contributed by electron transfer. Nie et al. also confirmed this view through experimental and theoretical calculations.[43] Nevertheless, it is noted that the rain droplets can also generate relatively high electricity (~0.5 μA and ~1.7 V), suggesting the viability of using the F-TENG as a potential energy harvesting rain coat. For all the above tests, the droplet fall height was 0.45 m. By increasing the height, the electrical output from raindrops can be further improved. As the fall height was increased from 0.2 to 1.25 m, the current increased from ~0.4 to ~6 μA, and the voltage increased from ~1.2 to ~4.3 V (Figure 2e). The higher fall heights will lead to the stronger impact force and higher sliding speed of the raindrops. Therefore, more electrified charges might be created under a higher impact force; in the meantime, the higher sliding speed means reduced time for charge transfer between the two electrodes and thus larger current. Lastly, we varied the incident angle of the raindrops. Four representative angles of 10, 30, 50, and 80° were set, and the rain fall height was 1.25 m. It was found that the output was high at 30 and 50° incident angles, but the output decreased significantly when the textile TENG was about perpendicular to (80°) or about parallel with (10°) the droplet fall direction (Figure S3).

The CS-TENG underneath the F-TENG is also able to harvest raindrop kinetic energies. The impact force produced when a raindrop falls onto the textile surface can result in the vertical contact-separation motions of the CS-TENG, as shown in Figure 3a. When the raindrops strike the top surface of the

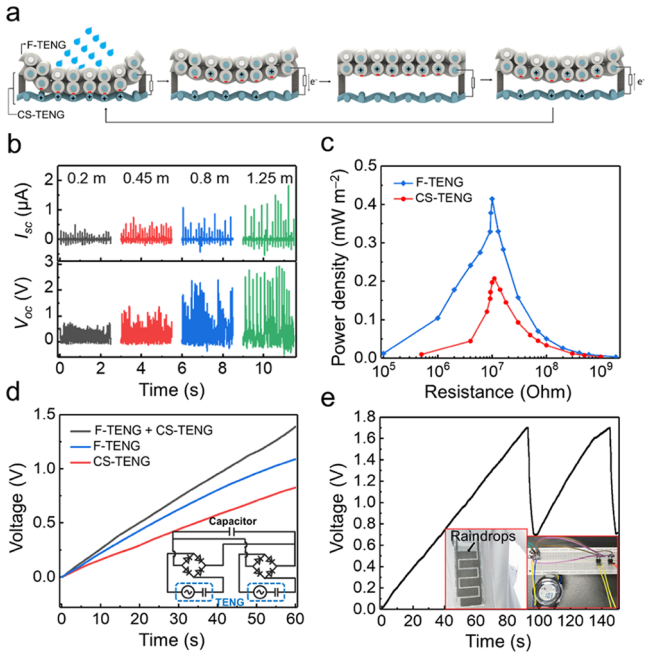

Figure 3. Harvesting raindrop energies by F-TENG and CS-TENG. (a) Schematic illustration of the working mechanism of the CS-TENG for harvesting raindrop energies. (b) Dependence of I_{sc} and V_{oc} on the raindrop falling height. (c) Comparison of the average output power density of F-TENG and CS-TENG for harvesting raindrop energies (1.25 m height). (d) Charging profiles of a 1 μF capacitor charged by dual-mode TENG, F-TENG, or CS-TENG. (e) Driving an electronic watch with the dual-mode TENG.

F-TENG, the underneath Parylene/Ni-coated textile will come in contact with the Ni-coated textile, leading to the generation of electrostatic negative charges in the Parylene coatings. When the two textiles bounce back to be separated, induced current flows through the external circuit to achieve local charge equilibrium. As the raindrops strike again, a reverse current pulse will be generated. Therefore, in an actual situation, the raindrop-induced vibration of the CS-TENG will lead to the AC electricity output. Similarly, the I_{sc} and V_{oc} increase with increasing raindrop fall height (Figure 3b). The current increased from ~0.25 to ~1.3 μA and the voltage increased from ~0.75 to ~2.9 V when the height increased from 0.2 to 1.25 m. The larger impact force certainly leads to the larger effective contacting area, more electrostatic charges, and therefore higher outputs. This also explains why higher outputs were obtained when the droplet incident angle was 80° (close to perpendicular), as shown in Figure S4.

The F-TENG and CS-TENG can be integrated in a parallel connection for harvesting raindrop energies. The F-TENG and CS-TENG exhibited a maximum output power of ~0.43 and ~0.22 mW m^{-2} ($P = U^2/RS$, where R is the resistance and S is the contacting surface area) at a matching resistance of 10 MΩ when the raindrop fall height was 1.25 m, respectively (Figure 3c). The generated electricity of the F-TENG and CS-TENG from raindrops can be utilized in charge capacitors with a rectifying circuit. A 1 μF capacitor can be charged to 0.8 and

https://doi.org/10.1021/acsami.1c03250
ACS Appl. Mater. Interfaces 2021, 13, 20145−20152

1.08 V by the CS-TENG and F-TENG in 60 s, respectively (Figure 3d). Nevertheless, the two generators connected in parallel can charge the capacitor to 1.35 V in 60 s, suggesting that both the raindrop striking and sliding motion energies are converted into electricity and are stored. After charging a 1 μF capacitor for 90 s, the voltage reaches 1.8 V and an electronic watch can be turned on for 8 s (Figure 3e).

2.3. Harvesting Wind Energies. The CS-TENG can scavenge wind energy, as the wind can also lead to vibration or contact-separation motions between the Parylene/Ni-coated textile and the Ni-coated textile, as shown in Figure 4a. The

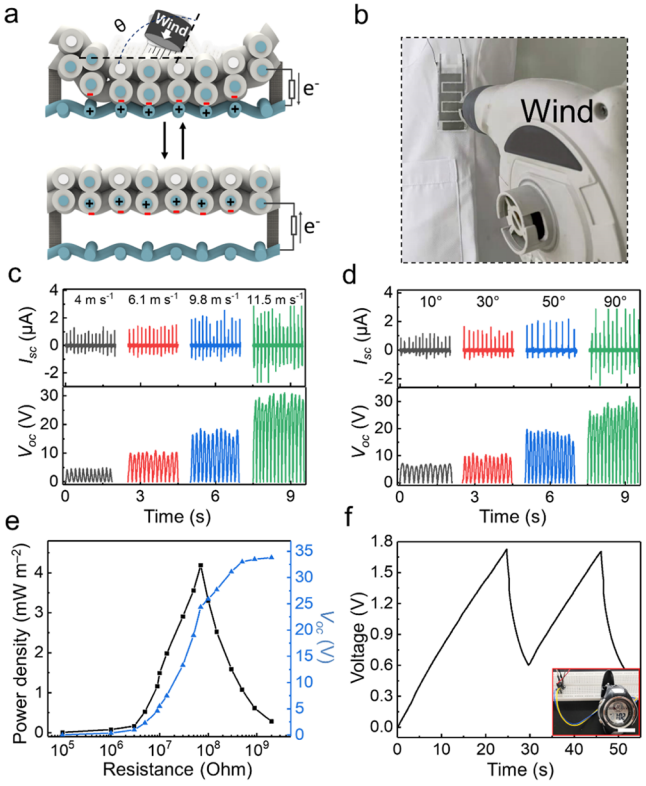

Figure 4. Harvesting wind energy. (a) Schematic illustration of CS-TENG for harvesting wind energy. (b) Photograph of the setup for the wind energy harvesting test. Dependence of I_{sc} and V_{oc} on (c) the wind velocity and (d) wind incident angles. (e) Average output power density of CS-TENG for harvesting wind energy (11.5 m s^{-1}). (f) Driving the electronic watch with the CS-TENG.

dynamic electricity generation process is similar to that in Figure 3a, but the raindrop impact changes to wind. Figure 4b shows the setup for the wind energy harvesting test, where the textile TENG was blown by a blower. The wind velocity and incident angle are the main parameters influencing the output performances because the vibration amplitude mainly depends on the intensity of the wind. The I_{sc} increased from ~1.0 to ~2.5 μA and V_{oc} increased from ~5 to ~30 V, as the wind speed increased from 4.0 to 11.5 m s^{-1} (Figure 4c). The outputs from the different wind direction (at 11.5 m s^{-1}) are illustrated in Figure 4d. Obviously, the wind blowing in the perpendicular direction generated the highest electricity output. Nevertheless, it was also confirmed that wind energy from arbitrary directions can be harvested by the CS-TENG, even though the output decreases when the wind direction is not perpendicular to CS-TENG. Compared with the previously reported wind energy TENGs,[12,34,44,45] this water-proof TENG can resist the failure caused by the rainy weather. The maximum peak output power of this CS-TENG can reach ~4.2 mW m^{-2} at a matched resistance of 70 MΩ under the wind speed of 11.5 m s^{-1}, as shown in Figure 4e. After charging a 1 μF capacitor by the CS-TENG (wind velocity 11.5 m s^{-1}) for only 24 s, the voltage reaches 1.7 V and the electronic watch can be powered for 6 s (Figure 4f).

2.4. Harvesting Human Motion Energies. Other than raindrop and wind energies, the CS-TENG can be readily used to collect kinetic energy from human motions. A linear motor was used to press the CS-TENG to mimic the possible pressure deformation induced by various body movements. Still, the dynamic electricity generation process is the same as that of raindrop- or wind-induced contact-separation motions of the CS-TENG, as shown in Figure 5a. As the pressure caused by human motions can be much larger than that of raindrops and wind, significantly higher outputs are expected. As for the CS-TENG, the spacer height (d) will affect the outputs. The relevant result is demonstrated in Figure S5. The V_{oc} increases with the d value, but when d exceeds 1.5 mm, the increase of V_{oc} becomes insignificant. Therefore, the d value should be at least 1.5 mm. Also, the d value we selected is 2 mm, because when applied to an actual operation, a lower spacer will make the separation insufficient, and a higher spacer will affect the flexibility of the textile.

When the pressure was 33 N and the motion frequency was 4 Hz, the output current reached ~15 μA and the voltage was over 120 V (Figure 5b). A maximum instantaneous power density of ~500 mW m^{-2} can be obtained at ~10 MΩ load (Figure 5c). In addition, no degradation of electric outputs was found after ~5000 times of contact-separation motions, confirming its excellent durability (Figure 5d). When worn underneath the arm, the CS-TENG can easily power 54 light-emitting diodes (LEDs) connected in series by pressing the textile TENG with the arm (Figure 5e). When swinging the arm naturally, the CS-TENG could produce V_{oc} to over 85 V, I_{sc} to over 9 μA, and Q_{sc} to over 27 nC (Figure S6a–c). Furthermore, the arm motions can charge a 33 μF capacitor to a voltage of 1.6 V in about 106 s, which can then power a calculator for about 13 s (Figure 5f).

Furthermore, the output performance of CS-TENG under various relative humidity conditions was tested (Figure S7). As the relative humidity increases from 20 to 90%, the initial output performance of CS-TENG decreases. As we know, TENG is based on the coupling of the tribsoelectrification effect and the electrostatic induction effect; once water molecules are adsorbed on the surface of the frictional layer, it will inevitably affect the process of charge generation.[46] Therefore, with the increase of relative humidity, the transferred charge decreases gradually and reaches a low equilibrium state eventually. The initial transferred charge of CS-TENG decreases from 64.5 to 39.7 nC (≈38.4% loss) when relative humidity increases from 20 to 90%. Hence, the surface charges can still be maintained at the higher equilibrium state under a high relative humidity environment. This further proves that the dual-mode TENG can simultaneously harvest multiple kinetic energies.

3. CONCLUSIONS

In summary, a textile TENG had been successfully fabricated for simultaneously harvesting kinetic energies from raindrops, winds, and human motions. A freestanding-mode textile TENG and a contact-separation-mode textile TENG were

https://doi.org/10.1021/acsami.1c03250
ACS Appl. Mater. Interfaces 2021, 13, 20145−20152

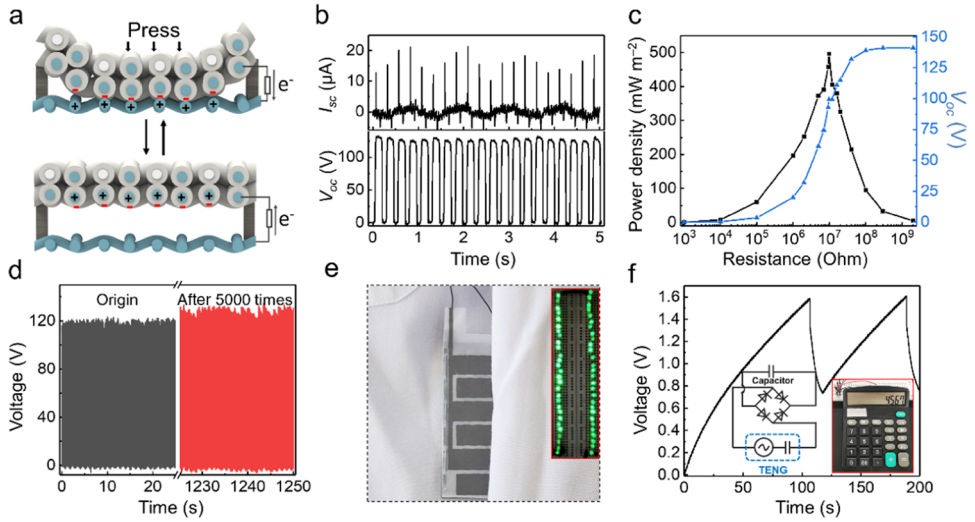

Figure 5. Harvesting human motion energy. (a) Schematic illustration of CS-TENG for harvesting human motion energy. (b) Generated I_{sc} and V_{oc} and (c) average output power density of CS-TENG (33 N, 4 Hz). (d) V_{oc} of CS-TENG before and after being continuously tested for 5000 cycles. (e) Photograph of the setup for human motion energy harvesting to drive 54 light-emitting diodes (LED). (f) Driving a calculator with the CS-TENG.

integrated together. The top surface of the textile TENG is hydrophobic and water repellent, making it suitable for harvesting raindrop kinetic energies. The freestanding-mode TENG was demonstrated to harvest the sliding kinetic energy of the raindrops, while the contact-separation-mode TENG was able to harvest the impact energy of raindrops. The structure parameters of the textile TENG were optimized to improve output performances. Furthermore, the contact-separation-mode TENG was demonstrated to harvest the energies of winds and human motions. Considering that the output of each TENG cannot be synchronized, the electrical output can be measured after the rectification circuit. The integrated TENG can simultaneously harvest multiple kinetic energies and store it in capacitors for powering small electronics. Therefore, we demonstrated a facile preparation of a TENG-based energy textile that can simultaneously harvest multiple kinetic energies.

4. EXPERIMENTAL SECTION

4.1. Fabrication of Textile F-TENG. To fabricate the F-TENG, polyester fabric was thoroughly cleaned with excess of acetone, alcohol, and deionized (DI) water by a bath sonicator, and then dried in a vacuum oven. Second, commercial polyester fabric stuck Kapton tapes on both sides were put under a computer-controlled commercial CO_2 laser for scribing the Kapton into interdigitated patterns. The intensity of the laser was regulated without damaging the sandwiched polyester fabric. Thereafter, the two interdigitated electrodes were electroless-deposited Ni on a polyester fabric, on top of which a Parylene film was conformally coated to serve as the tribo-electrification layer. The fabrication of this textile F-TENG was similar to our previous work.[25] Parylene (10 g) was coated using a chemical vapor deposition (CVD) method to prepare a transparent insulating coating with uniform thickness. To optimize the electrical output performances of F-TENG, the interval gap between adjacent finger electrodes was 2 mm to ensure electrical disconnection, while the width of a finger electrode unit was 8, 10, or 12 mm. Also, the total number (n) of electrode fingers of the two interdigitated electrodes was 2, 4, 6, or 8.

4.2. Fabrication of Textile CS-TENG. The CS-TENG underneath the F-TENG consists of two fabrics separated by a cotton fabric strip as the spacer. One of the fabrics is a conductive Ni-coated polyester textile; the other is a polyester textile coated with Ni and Parylene film successively. Also, the area of each piece was set as 20.3 cm^2. These F-TENGs and CS-TENG were sewed together with the F-TENG on the top.

4.3. Water Repellent Test. The water repellent property of the textile TENG was evaluated by putting a piece of weighed absorbent paper behind the textile, spraying a certain volume of water onto the surface of the textile, and then reweighing the absorbent paper. The average value of the three samples was determined by calculating the increase in the weight of the absorbent paper. If the value is greater than 5.0 g, it is recorded as 5+ g or >5.0 g. Before the test, the average value of the weight of the absorbent paper was 0.40 g, and then after the test, it was 0.41 g, which indicated an excellent water repellent property.

4.4. Characterizations and Measurements. A programmable electrometer (Keithley 6517) was used to measure the electrical output of the textile TENGs. Scanning electron microscopy (SEM) images were obtained with a Hitachi SU8020. The contact angle system OCA was used to measure the water contact angle of the Parylene/Ni-coated textile for characterizing its surface hydrophobicity. For performing the standard measurement of rain energy, the experiments involved spraying raindrops to a certain height through a self-made spray head. Furthermore, the rain water was home-made by mixing water, a small amount of sulfur dioxide, nitrogen dioxide, impurities, and floating dust, with the pH value being 5.7. A water repellent test of fabrics was based on the standard test method AATCC42-2007. For performing the standard measurement of wind energy, wind force was blown by a blower. An anemometer (TY826A) was applied to measure the wind speed. The TENGs were connected with a linear motor to mimic the movement of humans for the measurement. A force gauge (M5-50) was applied to measure the pressure.

■ ASSOCIATED CONTENT

Supporting Information

The Supporting Information is available free of charge at https://pubs.acs.org/doi/10.1021/acsami.1c03250.

Flexibility, softness, washability, and breathability of the dual-mode TENG (Figure S1); water repellent test of fabrics based on the AATCC42-2007 test method (Figure S2); generated I_{sc} and V_{oc} of F-TENG at different fall angles (Figure S3); generated I_{sc} and V_{oc} of CS-TENG at different fall angles (Figure S4); relation-

https://doi.org/10.1021/acsami.1c03250
ACS Appl. Mater. Interfaces 2021, 13, 20145−20152

ship between the spacer height (d) and the voltage output (Figure S5); generated I_{sc}, V_{oc}, and Q_{sc} from CS-TENG with an actual human motion (Figure S6); and open-circuit voltage and transferred charge of CS-TENG when changing ambient humidity (Figure S7) (PDF)

AUTHOR INFORMATION

Corresponding Authors

Xiong Pu − *School of Chemistry and Chemical Engineering, Center on Nanoenergy Research, School of Physical Science and Technology, Guangxi University, Nanning 530004, P. R. China; CAS Center for Excellence in Nanoscience, Beijing Key Laboratory of Micro-Nano Energy and Sensor, Beijing Institute of Nanoenergy and Nanosystems, Chinese Academy of Sciences, Beijing 101400, P. R. China; School of Nanoscience and Technology, University of Chinese Academy of Sciences, Beijing 100049, P. R. China;* orcid.org/0000-0002-1254-8503; Email: puxiong@binn.cas.cn

Zhong Lin Wang − *CAS Center for Excellence in Nanoscience, Beijing Key Laboratory of Micro-Nano Energy and Sensor, Beijing Institute of Nanoenergy and Nanosystems, Chinese Academy of Sciences, Beijing 101400, P. R. China; School of Nanoscience and Technology, University of Chinese Academy of Sciences, Beijing 100049, P. R. China; School of Materials Science and Engineering, Georgia Institute of Technology, Atlanta, Georgia 30332-0245, United States;* Email: zlwang@gatech.edu

Authors

Xuechao Gang − *School of Chemistry and Chemical Engineering, Center on Nanoenergy Research, School of Physical Science and Technology, Guangxi University, Nanning 530004, P. R. China; CAS Center for Excellence in Nanoscience, Beijing Key Laboratory of Micro-Nano Energy and Sensor, Beijing Institute of Nanoenergy and Nanosystems, Chinese Academy of Sciences, Beijing 101400, P. R. China*

Zi Hao Guo − *CAS Center for Excellence in Nanoscience, Beijing Key Laboratory of Micro-Nano Energy and Sensor, Beijing Institute of Nanoenergy and Nanosystems, Chinese Academy of Sciences, Beijing 101400, P. R. China; School of Nanoscience and Technology, University of Chinese Academy of Sciences, Beijing 100049, P. R. China*

Zifeng Cong − *CAS Center for Excellence in Nanoscience, Beijing Key Laboratory of Micro-Nano Energy and Sensor, Beijing Institute of Nanoenergy and Nanosystems, Chinese Academy of Sciences, Beijing 101400, P. R. China; School of Nanoscience and Technology, University of Chinese Academy of Sciences, Beijing 100049, P. R. China*

Jing Wang − *School of Chemistry and Chemical Engineering, Center on Nanoenergy Research, School of Physical Science and Technology, Guangxi University, Nanning 530004, P. R. China; CAS Center for Excellence in Nanoscience, Beijing Key Laboratory of Micro-Nano Energy and Sensor, Beijing Institute of Nanoenergy and Nanosystems, Chinese Academy of Sciences, Beijing 101400, P. R. China*

Caiyun Chang − *School of Chemistry and Chemical Engineering, Center on Nanoenergy Research, School of Physical Science and Technology, Guangxi University, Nanning 530004, P. R. China; CAS Center for Excellence in Nanoscience, Beijing Key Laboratory of Micro-Nano Energy and Sensor, Beijing Institute of Nanoenergy and Nanosystems, Chinese Academy of Sciences, Beijing 101400, P. R. China*

Chongxiang Pan − *School of Chemistry and Chemical Engineering, Center on Nanoenergy Research, School of Physical Science and Technology, Guangxi University, Nanning 530004, P. R. China; CAS Center for Excellence in Nanoscience, Beijing Key Laboratory of Micro-Nano Energy and Sensor, Beijing Institute of Nanoenergy and Nanosystems, Chinese Academy of Sciences, Beijing 101400, P. R. China*

Complete contact information is available at: https://pubs.acs.org/10.1021/acsami.1c03250

Notes

The authors declare no competing financial interest.

ACKNOWLEDGMENTS

The authors are grateful for the support from the National Key Research and Development Program of China (2016YFA0202702) and the Youth Innovation Promotion Association of CAS.

REFERENCES

(1) Wang, Z. L.; Song, J. Piezoelectric Nanogenerators Based on Zinc Oxide Nanowire Nrrays. *Science* **2006**, *312*, 242−246.

(2) Weng, W.; Chen, P.; He, S.; Sun, X.; Peng, H. Smart Electronic Textiles. *Angew. Chem., Int. Ed.* **2016**, *55*, 6140−6169.

(3) Shi, Q.; He, T.; Lee, C. More than Energy Harvesting − Combining Triboelectric Nanogenerator and Flexible Electronics Technology for Enabling Novel Micro-/Nano-Systems. *Nano Energy* **2019**, *57*, 851−871.

(4) Shi, Q.; Sun, J.; Hou, C.; Li, Y.; Zhang, Q.; Wang, H. Advanced Functional Fiber and Smart Textile. *Adv. Fiber Mater.* **2019**, *1*, 3−31.

(5) Lewis, N. S. Research Opportunities to Advance Solar Energy Utilization. *Science* **2016**, *351*, No. aad1920.

(6) Antonio, F. D. O. Wave Energy Utilization: A Review of the Technologies. *Renewable Sustainable Energy Rev.* **2010**, *14*, 899−918.

(7) Díaz-González, F.; Sumper, A.; Gomis-Bellmunt, O.; Villafáfila-Robles, R. A Review of Energy Storage Technologies for Wind Power Applications. *Renewable Sustainable Energy Rev.* **2012**, *16*, 2154−2171.

(8) Wang, Z. L. Entropy Theory of Distributed Energy for Internet of Things. *Nano Energy* **2019**, *58*, 669−672.

(9) Chen, X.; Xiong, J.; Parida, K.; Guo, M.; Wang, C.; Wang, C.; Li, X.; Shao, J.; Lee, P. S. Transparent and Stretchable Bimodal Triboelectric Nanogenerators with Hierarchical Micro-Nanostructures for Mechanical and Water Energy Harvesting. *Nano Energy* **2019**, *64*, No. 103904.

(10) Lin, Z. H.; Cheng, G.; Lin, L.; Lee, S.; Wang, Z. L. Water-Solid Surface Contact Electrification and its Use for Harvesting Liquid-Wave Energy. *Angew. Chem., Int. Ed.* **2013**, *52*, 12545−12549.

(11) Ye, C.; Xu, Q.; Ren, J.; Ling, S. Violin String Inspired Core-Sheath Silk/Steel Yarns for Wearable Triboelectric Nanogenerator Applications. *Adv. Fiber Mater.* **2020**, *2*, 24−33.

(12) Zhao, Z.; Pu, X.; Du, C.; Li, L.; Jiang, C.; Hu, W.; Wang, Z. L. Freestanding Flag-Type Triboelectric Nanogenerator for Harvesting High-Altitude Wind Energy from Arbitrary Directions. *ACS Nano* **2016**, *10*, 1780−1787.

(13) Wang, S.; Lin, L.; Wang, Z. L. Triboelectric Nanogenerators as Self-Powered Active Sensors. *Nano Energy* **2015**, *11*, 436−462.

(14) Zi, Y.; Guo, H.; Wen, Z.; Yeh, M. H.; Hu, C.; Wang, Z. L. Harvesting Low-Frequency (<5 Hz) Irregular Mechanical Energy: A Possible Killer Application of Triboelectric Nanogenerator. *ACS Nano* **2016**, *10*, 4797−4805.

(15) Sun, J.; Pu, X.; Liu, M.; Yu, A.; Du, C.; Zhai, J.; Hu, W.; Wang, Z. L. Self-Healable, Stretchable, Transparent Triboelectric Nanogenerators as Soft Power Sources. *ACS Nano* **2018**, *12*, 6147−6155.

(16) Zhang, P.; Chen, Y.; Guo, Z. H.; Guo, W.; Pu, X.; Wang, Z. L. Stretchable, Transparent, and Thermally Stable Triboelectric Nano-

generators Based on Solvent-Free Ion-Conducting Elastomer Electrodes. *Adv. Funct. Mater.* **2020**, *30*, No. 1909252.
(17) Li, J.; Sun, J.; Wu, D.; Huang, W.; Zhu, M.; Reichmanis, E.; Yang, S. Functionalization-Directed Stabilization of Hydrogen-Bonded Polymer Complex Fibers: Elasticity and Conductivity. *Adv. Fiber Mater.* **2019**, *1*, 71−81.
(18) Liu, Y.; Liu, W.; Wang, Z.; He, W.; Tang, Q.; Xi, Y.; Wang, X.; Guo, H.; Hu, C. Quantifying Contact Status and the Air-breakdown Model of Charge-excitation Triboelectric Nanogenerators to Maximize Charge Density. *Nat Commun* **2020**, *11*, No. 1599.
(19) Wang, Z.; Liu, W.; He, W.; Guo, H.; Long, L.; Xi, Y.; Wang, X.; Liu, A.; Hu, C. Ultrahigh Electricity Generation from Low-Frequency Mechanical Energy by Efficient Energy Management. *Joule* **2021**, *5*, 441−455.
(20) Xiong, J.; Lee, P. S. Progress on Wearable Triboelectric Nanogenerators in Shapes of Fiber, Yarn, and Textile. *Sci. Technol. Adv. Mater.* **2019**, *20*, 837−857.
(21) Xiong, J.; Cui, P.; Chen, X.; Wang, J.; Parida, K.; Lin, M. F.; Lee, P. S. Skin-Touch-Actuated Textile-based Triboelectric Nanogenerator with Black Phosphorus for Durable Biomechanical Energy Harvesting. *Nat. Commun.* **2018**, *9*, No. 4280.
(22) Kwak, S. S.; Yoon, H.-J.; Kim, S.-W. Textile-Based Triboelectric Nanogenerators for Self-Powered Wearable Electronics. *Adv. Funct. Mater.* **2019**, *29*, No. 1804533.
(23) Liu, M.; Pu, X.; Jiang, C.; Liu, T.; Huang, X.; Chen, L.; Du, C.; Sun, J.; Hu, W.; Wang, Z. L. Large-Area All-Textile Pressure Sensors for Monitoring Human Motion and Physiological Signals. *Adv. Mater.* **2017**, *29*, No. 1703700.
(24) Pu, X.; Li, L.; Liu, M.; Jiang, C.; Du, C.; Zhao, Z.; Hu, W.; Wang, Z. L. Wearable Self-Charging Power Textile Based on Flexible Yarn Supercapacitors and Fabric Nanogenerators. *Adv. Mater.* **2016**, *28*, 98−105.
(25) Pu, X.; Li, L.; Song, H.; Du, C.; Zhao, Z.; Jiang, C.; Cao, G.; Hu, W.; Wang, Z. L. A self-Charging Power Unit by Integration of a Textile Triboelectric Nanogenerator and a Flexible Lithium-ion Battery for Wearable Electronics. *Adv. Mater.* **2015**, *27*, 2472−2478.
(26) Pu, X.; Liu, M.; Li, L.; Han, S.; Li, X.; Jiang, C.; Du, C.; Luo, J.; Hu, W.; Wang, Z. L. Wearable Textile-Based In-Plane Microsupercapacitors. *Adv. Energy Mater.* **2016**, *6*, No. 1601254.
(27) Yu, A.; Pu, X.; Wen, R.; Liu, M.; Zhou, T.; Zhang, K.; Zhang, Y.; Zhai, J.; Hu, W.; Wang, Z. L. Core-Shell-Yarn-Based Triboelectric Nanogenerator Textiles as Power Cloths. *ACS Nano* **2017**, *11*, 12764−12771.
(28) Chen, J.; Huang, Y.; Zhang, N.; Zou, H.; Liu, R.; Tao, C.; Fan, X.; Wang, Z. L. Micro-Cable Structured Textile for Simultaneously Harvesting Solar and Mechanical Energy. *Nat. Energy* **2016**, *1*, No. 16138.
(29) Wen, Z.; Yeh, M. H.; Guo, H.; Wang, J.; Zi, Y.; Xu, W.; Deng, J.; Zhu, L.; Wang, X.; Hu, C.; Zhu, L.; Sun, X.; Wang, Z. L. Self-powered Textile for Wearable Electronics by Hybridizing Fiber-Shaped Nanogenerators, Solar Cells, and Supercapacitors. *Sci. Adv.* **2016**, *2*, No. e1600097.
(30) Lin, M.-F.; Parida, K.; Cheng, X.; Lee, P. S. Flexible Superamphiphobic Film for Water Energy Harvesting. *Adv. Mater. Technol.* **2017**, *2*, No. 1600186.
(31) Wang, H.; Wu, H.; Hasan, D.; He, T.; Shi, Q.; Lee, C. Self-Powered Dual-Mode Amenity Sensor Based on the Water-Air Triboelectric Nanogenerator. *ACS Nano* **2017**, *11*, 10337−10346.
(32) Kil Yun, B.; Soo Kim, H.; Joon Ko, Y.; Murillo, G.; Hoon Jung, J. Interdigital Electrode Based Triboelectric Nanogenerator for Effective Energy Harvesting from Water. *Nano Energy* **2017**, *36*, 233−240.
(33) Kim, K. N.; Chun, J.; Kim, J. W.; Lee, K. Y.; Park, J.-U.; Kim, S.-W.; Wang, Z. L.; Baik, J. M. Highly Stretchable 2D Fabrics for Wearable Triboelectric Nanogenerator under Harsh Environments. *ACS Nano* **2015**, *9*, 6394−6400.
(34) Lai, Y. C.; Hsiao, Y. C.; Wu, H. M.; Wang, Z. L. Waterproof Fabric-Based Multifunctional Triboelectric Nanogenerator for Universally Harvesting Energy from Raindrops, Wind, and Human Motions and as Self-Powered Sensors. *Adv. Sci.* **2019**, *6*, No. 1801883.
(35) Lin, S.; Zheng, M.; Luo, J.; Wang, Z. L. Effects of Surface Functional Groups on Electron Transfer at Liquid-Solid Interfacial Contact Electrification. *ACS Nano* **2020**, *14*, 10733−10741.
(36) Zhan, F.; Wang, A. C.; Xu, L.; Lin, S.; Shao, J.; Chen, X.; Wang, Z. L. Electron Transfer as a Liquid Droplet Contacting a Polymer Surface. *ACS Nano* **2020**, *14*, 17565−17573.
(37) Zhang, L.; Li, X.; Zhang, Y.; Feng, Y.; Zhou, F.; Wang, D. Regulation and Influence Factors of Triboelectricity at the Solid-Liquid Interface. *Nano Energy* **2020**, *78*, No. 105370.
(38) Lin, S.; Xu, L.; Chi Wang, A.; Wang, Z. L. Quantifying Electron-Transfer in Liquid-Solid Contact Electrification and the Formation of Electric Double-Layer. *Nat. Commun.* **2020**, *11*, No. 399.
(39) Burgo, T. A. L.; Galembeck, F.; Pollack, G. H. Where is Water in the Triboelectric Series? *J. Electrost.* **2016**, *80*, 30−33.
(40) Wang, Z. L. Triboelectric Nanogenerators as New Energy Technology and Self-Powered Sensors - Principles, Problems and Perspectives. *Faraday Discuss.* **2014**, *176*, 447−458.
(41) Park, H.-Y.; Kim, H. K.; Hwang, Y.-H.; Shin, D.-M. Water-Through Triboelectric Nanogenerator Based on Ti-Mesh for Harvesting Liquid Flow. *J. Korean Phys. Soc.* **2018**, *72*, 499−503.
(42) Zhao, L.; Liu, L.; Yang, X.; Hong, H.; Yang, Q.; Wang, J.; Tang, Q. Cumulative Charging Behavior of Water Droplet Driven Freestanding Triboelectric Nanogenerators toward Hydrodynamic Energy Harvesting. *J. Mater. Chem. A* **2020**, *8*, 7880−7888.
(43) Nie, J.; Ren, Z.; Xu, L.; Lin, S.; Zhan, F.; Chen, X.; Wang, Z. L. Probing Contact-Electrification-Induced Electron and Ion Transfers at a Liquid-Solid Interface. *Adv. Mater.* **2020**, *32*, No. 1905696.
(44) Yang, Y.; Zhu, G.; Zhang, H.; Chen, J.; Zhong, X.; Lin, Z. H.; Su, Y.; Bai, P.; Wen, X.; Wang, Z. L. Triboelectric Nanogenerator for Harvesting Wind Energy and as Self-Powered Wind Vector Sensor System. *ACS Nano* **2013**, *7*, 9461−9468.
(45) Zhang, L.; Zhang, B.; Chen, J.; Jin, L.; Deng, W.; Tang, J.; Zhang, H.; Pan, H.; Zhu, M.; Yang, W.; Wang, Z. L. Lawn Structured Triboelectric Nanogenerators for Scavenging Sweeping Wind Energy on Rooftops. *Adv. Mater.* **2016**, *28*, 1650−1656.
(46) Li, L.; Wang, X.; Zhu, P.; Li, H.; Wang, F.; Wu, J. The Electron Transfer Mechanism Between Metal and Amorphous Polymers in Humidity Environment for Triboelectric Nanogenerator. *Nano Energy* **2020**, *70*, No. 104476.

https://doi.org/10.1021/acsami.1c03250
ACS Appl. Mater. Interfaces 2021, 13, 20145−20152